Electronic Supplementary Material (ESI) for Green Chemistry.

Supporting Information

Highly Selective Electrocatalytic Oxidation of Benzyl C−H Using Water as Safe and Sustainable Oxygen Source

Yuxia Sun, Xiaoshan Li, Miao Yang, Wentao Xu, Jin Xie, and Mengning Ding *

Table of Contents

1. Experimental Procedures

1.1 Preparation of anodic materials

1.2 General characterizations and measurements

1.3 Electrochemical methods

1.4 Product analysis

2. Results and Discussion

2.1. Comparison of different additives, potential and cathodes for the electro-oxidation of THN

2.2. Control experiments for the possible pathway and oxidants of electro-oxidation of THN

2.3. The measurements for exploring the process of electro-oxidation of THN.

2.4. The IR spectra of treated carbon paper

2.5. SEM, TEM images and XRD patterns of prepared MnO_2 catalysts for electro-oxidation of THN

2.6. The ECSA measurement of MnO_2 and MnO2-N_2

2.7. Comparison of different anode materials for the electro-oxidation of THN

2.8 Characterization of catalyst after reaction

2.9 CV plots of THN in different systems

2.10 The GC detection of O_2 gas in the system

2.11 The set up of the electrochemical cells

2.12 Information of isolated benzyl compounds

3. References

1. Experimental Procedures

1.1 Preparation of anodic materials

Preparation of Fenton-treated carbon paper. In a typical preparation, a 1×1 cm carbon paper was placed in $FeSO_4$ aqueous solution (1.0 g $FeSO_4 \cdot 4H_2O$ dissolved in 10 mL of DI H_2O), then 15 ml of H_2O_2 (30% wt) was added dropwise to the solution under vigorous agitation. After stirring for 3 h, the treated carbon paper was taken out and washed by 3 M HCl aqueous solution and deionized water (MiliQ) until the supernatant was neutral, followed by drying at 70 °C overnight under vacuum. The obtained carbon paper was denoted as Fenton-Hydrophilic CP.

Preparation of layered MnO_2 and MnO_2-N_2: The preparation was based on a process of solid interface reaction.[1] In a typical process, 0.5 mmol finely powdered $KMnO_4$ and 0.75 mmol finely powdered $Mn(OAc)_2$ were mixed in an agate mortar. After fully ground for about 15 min, the converted material was washed several times with ethanol and separated by centrifugation. Then, the obtained sample was dried under vacuum overnight and labelled as MnO_2. MnO_2-N_2 was prepared by treatment of MnO_2 under flow N_2 in a tubular furnace. It was heated to 200 °C (at 5 °C/min rate) and kept for 2 h under N_2 with a flow rate of 40ml/min.

Preparation of MnO_2-CP or MnO_2 (N_2-Treated)/CP anodes: The catalyst inks were prepared by adding 2.5 mg mL^{-1} MnO_2-CP or MnO_2 (N_2-Treated) to a solution consisting of 48 vol% water, 48 vol% ethanol and 2 vol% Nafion (5% w/w solution, Alfa Aesar). After sonicating the mixture for 30 min, 120 μL of the ink were drop-cast onto the normal CP and dried under an infrared lamp.

1.2 General Characterization

XRD patterns were recorded on a Shimadzu Lab X/XRD-6000 X-ray diffractometer equipped with a Cu-Kα radiation source (λ= 0.15418 nm) operating at 40 kV and 30 mA. SEM image were recorded on Hitachi S-4800 with samples deposited on carbon conductive tapes. TEM and High-resolution TEM images were obtained on JEOL JEM-1011 and JEM-2100 with samples deposited on carbon coated Cu grids, respectively. The Fourier Transform infrared spectroscopy (FT-IR) measurements were proceeded on a Bruker VERTEX 70 at a resolution of 4 cm^{-1}. X-ray photoelectron spectroscopy (XPS) was performed on a UlVAC-PHI 5000 Versa Probe spectrometer with Al Kα as radiation source. The binding energies in recorded spectra were calibrated by the C 1s peak, the internal standard reference at 284.6 eV. Electron spin resonance (ESR) spectra were obtained using a Bruker ESR spectrometer (Bruker EMXplus, 300 K, 19.12 mW, 9.8528 GHz). Raman spectrum was collected at room temperature on a Horib France Sas Xplora Plus Raman spectroscope equipped with a 532 nm laser source.

1.3 Electrochemical methods

Electrochemical experiments were conducted in an undivided electrochemical cell with a standard three-electrode system using a Corrtest CS3004 electrochemical workstation. Platinum foil and glass carbon electrode (3mm diameter)/RVC/carbon paper (1×1 cm) were used as the counter and working electrode, respectively (Figure S1，glass carbon was the working electrode). An Ag/Ag^+ electrode (10 mmol/L $AgNO_3$) was used as the reference electrode and connected with the reaction system with a L-type salt bridge, which avoided possible constituent change in the reference. The potentials were calibrated by measuring the reversible redox pair Fc/Fc^+ (10 mM ferrocene / ferrocenium). To determine the effect of water addition on the anode oxidation of tetralin, cyclic voltammetry (CV) curves were recorded using glass carbon as the working electrode. To testify the catalytic activity of prepared MnO_2 towards tetralin activation, CV curves were recorded using MnO_2-loaded carbon paper (1×1 cm). Acetonitrile with 0.1 M tetrabutylammonium perchlorate (Bu_4NClO_4) was used as the solvent with varying fraction of water. Total volume of electrolyte was set to be 25 mL. All the potentials were not IR compensated manually. For each bulk electrolysis measurement, 25 mL of electrolyte containing a specified amount of tetraline, water, and acetonitrile was added into the undivided cell and a micro-magnetic spin bar was placed into the cell for stirring. For the cyclic voltammetry analysis, CV scans were initiated from the open-circuit potential, and ten cycles were recorded successively at a scan rate of 100 mV/sec. To obtain electro-kinetic data in Figure 4b, the chronoamperometry analysis was conducted at 1.65 V vs Ag/Ag^+ (1.55 V vs Fc/Fc^+). In a typical CV measurement, the potentials were scanned for several cycles (~5) until a stable current is achieved, after which the final CV result was acquired.

To elucidating the prior selection of undivided cell, a set of control experiments were carried out. First, in a divided cell with proton exchange membrane, THN was placed in the anodic cell while other conditions were kept the same. GC results revealed that the THNO yield was about half of the that from undivided cell. Moreover, we noticed that the electrical resistance (measured by potentiostat) was 10 times higher in the divided cell. Secondly, in a divided cell, both reactant THN and product TONE were added in the cathode side, and

kept at the same potential for 9 h. GC analysis showed no obvious change in concentration for both THN and TONE. This result shows that the reduction of organic substances formed at anode side did not occur on the cathode, which is probably not thermodynamically preferred compared to HER. That is, the use of undivided cell will not cause side reactions and can minimize the internal resistance in the system, making the setup of undivided cell reasonable..

Electrochemical Surface Area(ECSA) is a general alternative methodology to characterize the amounts of active sites. The capacitance of the double layer Cdl is commonly used to estimate the effective ECSA, assuming that the two quantities are linearly proportional. Cyclic voltammetry can be used as a simple method to determine the Cdl. The CV measurements were carried out on in the region of -0.18–0.02 V vs. Fc/Fc^+, where the currents are mostly due to the charging of the double layer. The capacitance of the catalyst can be calculated from the scan rate dependence of charging current density at E =0.08 V vs. Fc/Fc^+, where the slope of the ΔJ vs. scan rate curve is twice the C_{dl}.

1.4 Product analysis

Gas chromatography measurements were carried out on Shimadzu Nexis GC-2030 with a flame ionization detector and SH-Rtx-1 capillary column (30 m, 0.25 mm ID, 0.25 μm df) for separation of reaction mixtures. The temperature of the column was initially kept at 70 ºC for 1 min and first increased to 150 ºC at a rate of 10 ºC/min. Then the temperature was increased to 250 ºC at a rate of 25 ºC/min and kept for 3 min. Dodecane was used as the internal standard to quantify the substrate and products. The conversion of THN and the yields were calculated as follows;

Conversion= (1- moles of THN /moles of THN loaded) ×100%

Yield= (moles of product/moles of THN loaded) ×100%

FE Determination: A sealed undivided electrochemical cell was used (one hole was sealed with PTFE/silicone rubber septa, similar to Gas Chromatography septa). A Hamilton gastight syringe was used to collect the H_2 gas. The quantification of H_2 was carried out by Gas chromatography on Shimadzu Nexis GC-2030 with a thermal conductivity detector and SH-Rt®-Msieve column (30 m, 0.53 mm ID, 50 μm DF). The temperature of spli was 50 ºC; the column was kept at 40 ºC for 3 min; the detector temperature was 150 ºC and the bridge current was set to be 40 mA. The quantitation was based on the standard curve shown in Figure S2. The Faraday for TONE and H_2 production were calculated as follows.

FE_{TONE}(%) = mol of TONE/[total passed charge/(4 × F)]×100%

FE_{H2}(%) = mol of hydrogen/[total passed charge/(2 × F)]×100%”

O_2 Detection: A sealed electrochemical undivided cell was used, and the inlet and outlet pipe with Ar Flow at 30 cc/min was set to take out the overhead gas component in the cell for quantitiative detection. The analysis was carried out by Gas chromatography on GC-9860-5C-NJ with a thermal conductivity detector and JN. Al_2O_3 column (30 m, 0.53 mm ID) along the reaction process. GC conditions: the temperature of spli was 220 ºC; the column was kept at 60 ºC for 6 min; the detector temperature was 120 ºC and the bridge current was set to be 75 mA.

2. Results and Discussion

2.1 Comparison of different additives, potential and cathodes for the electro-oxidation of THN.

Table S1. Comparison of different additives for the electro-oxidation of THN[a].

Entry	Solvent	Electrolyte	Additive(Amount (mmol))	Conv. (%)	Yield of TONE (%)	Yield of TOL (%)
1	CH_3CN	Bu_4NClO_4	-	94.8	15.9	n.d.
2	CH_3CN/H_2O (99/1)	Bu_4NClO_4	-	98.3	7.6	n.d.
3	CH_3CN/H_2O (85/15)	Bu_4NClO_4	-	82.6	19.8	n.d.
4	CH_3CN/H_2O (30/70)	Bu_4NClO_4	-	59.7	6.5	n.d.
5	CH_3CN/H_2O (90/10)	$LiBF_4$	-	≥99	55.4	n.d.
6	CH_3CN/H_2O (90/10)	$LiSO_3CF_3$	-	98.6	36.5	n.d.
7	CH_3CN/H_2O (90/10)	SDS	-	47.5	8.4	n.d.
5	CH_3CN/H_2O (90/10)	Bu_4NBF_4	-	31.2	8.9	n.d.
8[b]	CH_3CN/H_2O (90/10)	Bu_4NClO_4	NaOAc (0.25)	98.6	36.5	n.d.
9[b]	CH_3CN/H_2O (90/10)	Bu_4NClO_4	NaOAc(0.5)	≥99	55.4	n.d.
10[b]	CH_3CN/H_2O (90/10)	Bu_4NClO_4	$HClO_4$(0.1)	87.9	25.5	25.5
11[b]	CH_3CN/H_2O (90/10)	Bu_4NClO_4	NaOH($6*10^{-5}$)	82.1	15.2	24.2

[a] Reaction conditions: 0.65 mmol tetralin, RVC-Pt, 25 mL solvent, electrolyte (0.1 M), 12 h, applied potential: 1.75 V vs Fc/ Fc^+; TONE and TOL are the abbreviation for 1-tetralone and 1-tetralol, respectively. [b] Reaction time: 6h.

Table S2. Comparison of different applied potential and cathodes for the electro-oxidation of THN[a].

Entry	Cathode	Potential (V)	Yield of TONE (%)	Conv. (%)
1	Pt	1.45	34.1	94.1
2	Pt	1.55	45.9	≥99
3	Pt	1.65	43.0	≥99
4	Pt	1.75	62.0	>99
5	RVC	1.75	25.3	98.3
6	Pt	18 mA	23.3	85.2

[a] Reaction conditions: 0.65 mmol tetralin, RVC (anode), 25 mL solvent (CH_3CN/H_2O=90/10)), electrolyte (0.1 M Bu_4NClO_4), additive (NaOAc), 12 h; potentials were calibrated by Fc/Fc^+; TONE is the abbreviation for tetralone.

2.2 Control experiments for the possible pathway and oxidants of electro-oxidation of THN.

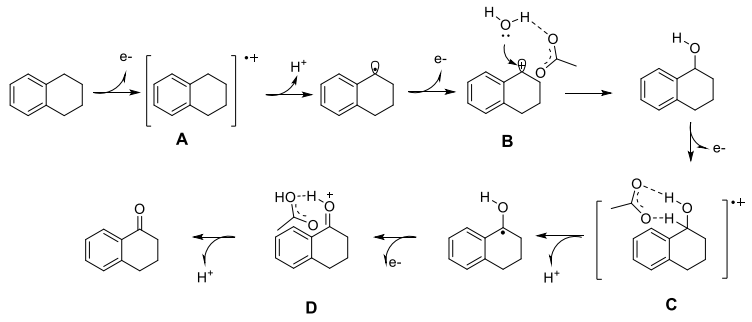

Scheme S1. Plausible Reaction Pathway.

NaOAc presumablely functions as a Brønsted base. In the reaction process, THN is first oxidized at the anode, producing a radical cation intermediate A. After consequent deprotonation and a second electron transfer process, cation B is formed, which is attacked by H_2O promoted by Bronsted base NaOAc. The deprotonation of intermediate might also be promoted by Bronsted base NaOAc;

For the MnO_2 case, it could assume a possible in the stabilization of cationic intermediates (probably through the chemical adsorption similar to OER case), also help the deprotonation of water molecules via a mechanism similar to OER process (in OER mechanism, two water molecules were chemically adsorbed on the adjacent MnIII/IV centers, one of them can be replaced by THN molecule that lead to the onsite formation of cationic intermediate)

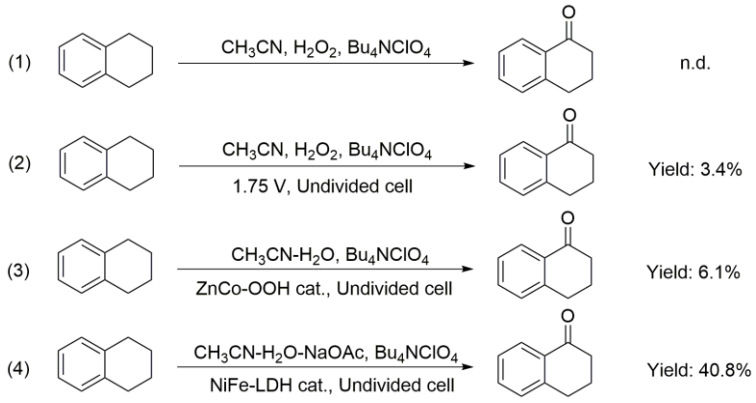

Scheme S2. (1) Control experiments with H_2O_2 as the oxidant. (2) Control experiments with H_2O_2 as the oxidant with applied voltage 1.75 V vs Fc^+/ Fc. (3) Control experiments with Zn-Co-OOH and NiFe-LDH as the catalyst with applied voltage 1.75 V vs Fc/ Fc^+.

2.3 The measurements for exploring the process of electro-oxidation of THN.

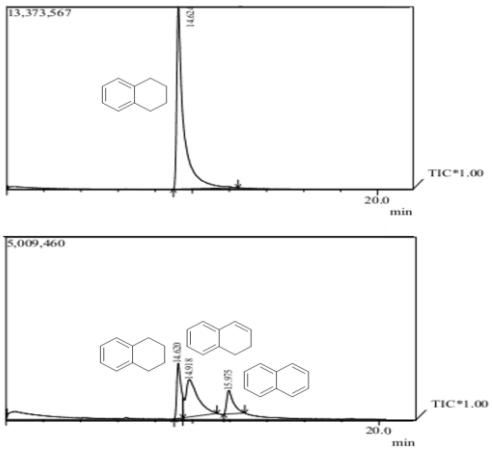

Figure S1. The GC chromatography for THN and dehydrogenation products of THN .

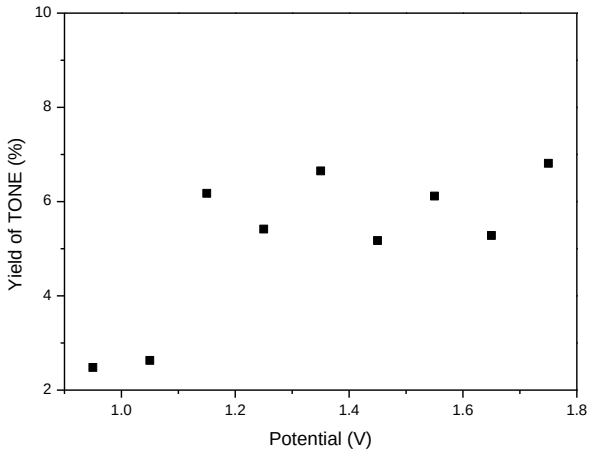

Figure S2. The Yield of TONE at different potentials at Q=35 C.

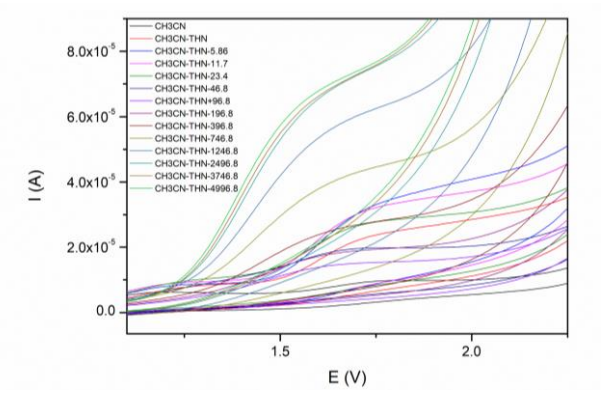

Figure S3. CV of THN in CH_3CN-H_2O system with different amount of water (The numbers inset were the added amount). Electrolyte (Bu_4NClO_4, 0.1 M), solvent (25 mL, the numbers inset were the water amount (μl)), electrode (GC), the potential was calibrated by Fc/Fc^+.

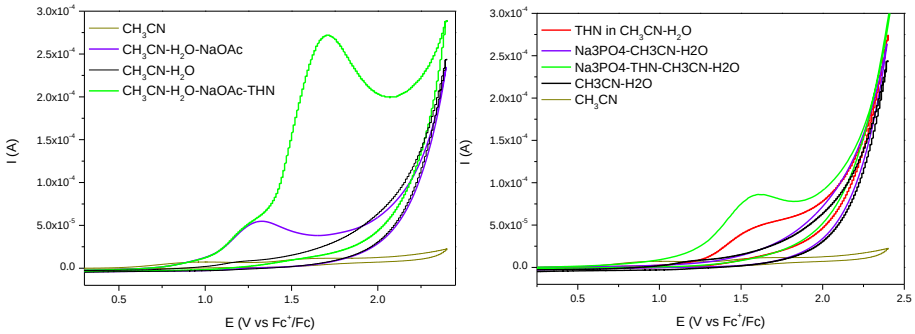

Figure S4. (a) CV of CH_3CN (dark yellow), CH_3CN-H_2O (black), NaOAc in CH_3CN-H_2O (violet) and THN-NaOAc in CH_3CN-H_2O system (green). (b) CV of CH_3CN (dark yellow), CH_3CN-H_2O (black), Na_3PO4 in CH_3CN-H_2O (violet), THN in CH_3CN-H_2O (red) and THN-Na_3PO_4 in CH_3CN-H_2O system (green).

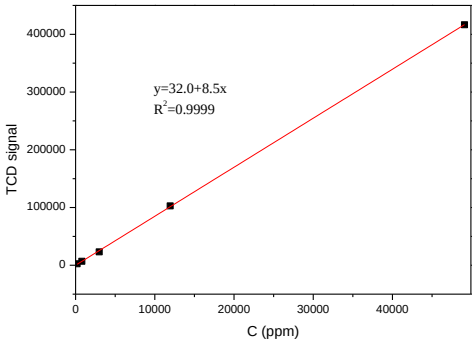

Figure S5. The standard curve of TCD signal dependence on H_2 concentration for quantitation.

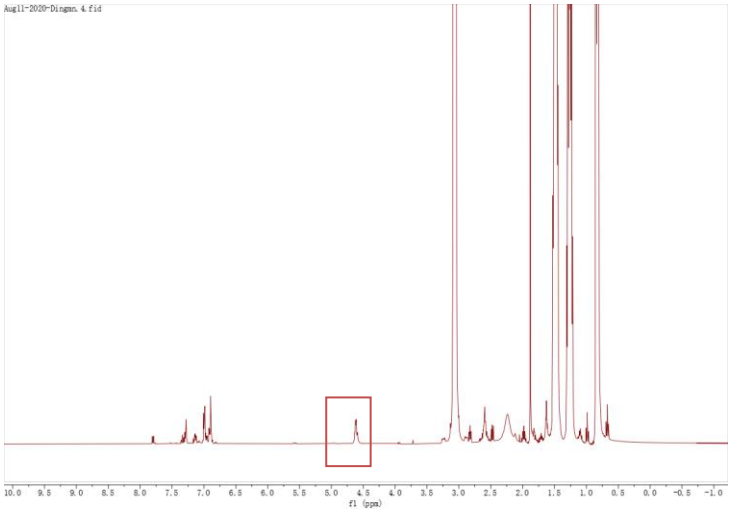

Figure S6. The NMR spectra of the sample taking from the electro-oxidation system at 15 min.

Different from THN and TONE, characteristic 1H shift of 1-tetralol (TOL) at near 4.75 ppm

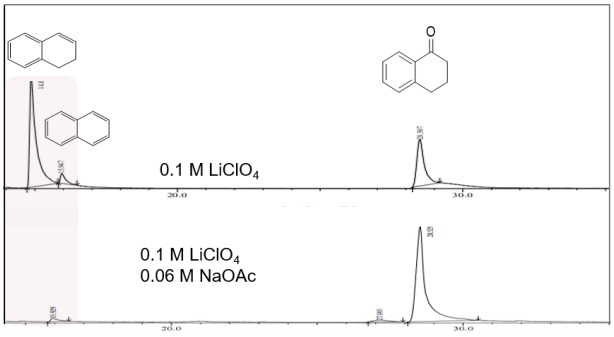

Figure S7. The GC chromatography for electro-oxidation with 1-tetralol **(**TOL**)** as the substrate.

Reaction conditions: 0.65 mmol TOL, RVC-Pt, 25 mL solvent CH_3CN-H_2O (90:10), 12 h, applied potential: 1.75 V vs Fc/ Fc^+.

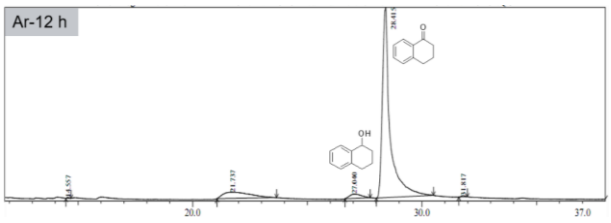

Figure S8. The GC chromatography for THN electro-oxidation under Ar atmosphere.

Reaction conditions: 0.65 mmol THN, RVC-Pt, 25 mL solvent CH_3CN-H_2O (90:10), 12 h, Ar atmosphere, applied potential: 1.75 V vs Fc/ Fc^+.

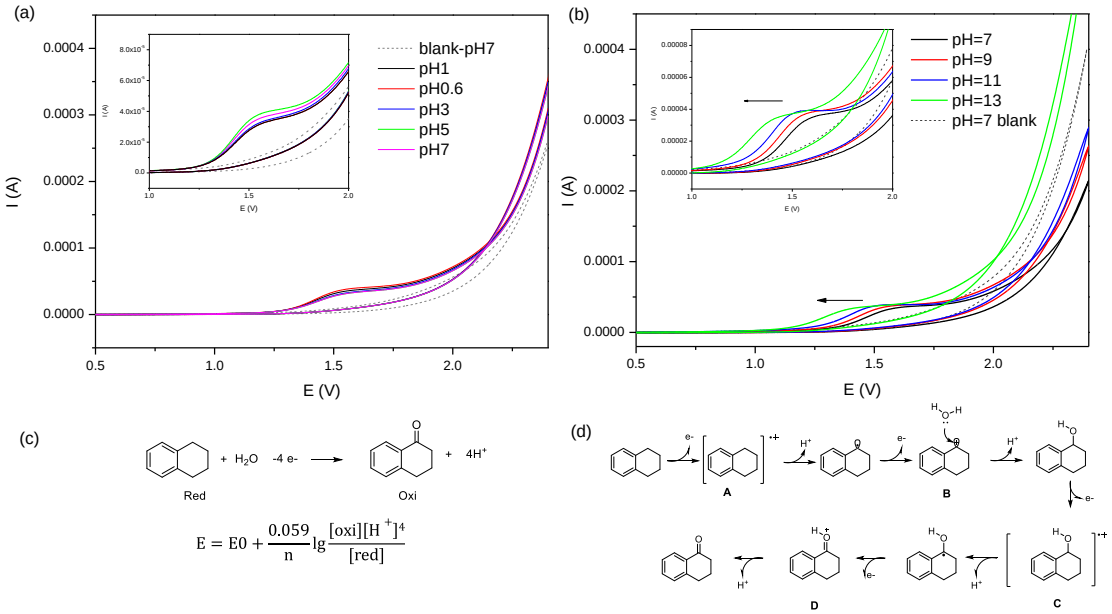

Figure S9. CV of THN in CH_3CN-H_2O system with different pH

Electrolyte (Bu_4NClO_4, 0.1 M), solvent (25 mL, CH_3CN/H_2O=90/10), electrode (Glass carbon, d= 3 mm). Basicity adjusted by NaOH, acidity adjusted by $HClO_4$.

The CV scans of reaction system under different pH were collected under identical conditions. In alkaline electrolyte, the onset potential presented a negative shift with higher pH, consistent with the predicted trend by Nernst Equation E= E0 - 0.0591pH. However, the value of ~0.03 in our system,is smaller than 0.0591 because the electroorganic oxidation is generally an irreversible electrochemical process. Interestingly, in the acidic electrolyte, we did not observe the same trend, and the CV curves did not demonstrate significant change with varying pH value. The different CV behaviors under alkaline or acidic electrolytes indicate that in our electrochemical oxidation of THN to TONE in mixed organic-water solvent, the rate determining step might be different in alkaline and acidic conditions

2.4 The IR spectra of treated carbon paper

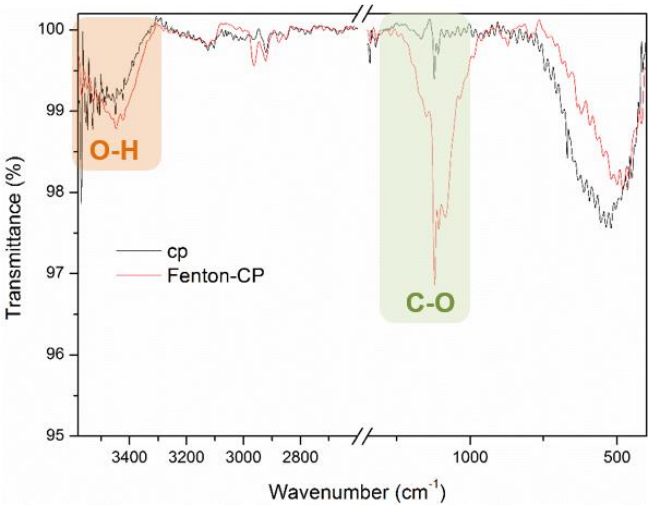

Figure S10. The FT-IR spectra of Fenton-treated carbon paper.

After Fenton oxidative treatment to carbon paper, the IR spectrum of Fenton-CP suggested that a large amount of -O-H and C-O groups were formed on the surface. The intermolecular hydrogen bonds between the surface functional groups and water molecules may contribute to the super-hydrophilicity of Fenton-CP.

2.5 The SEM, TEM and XRD patterns of prepared MnO_2 catalysts for electro-oxidation of THN.

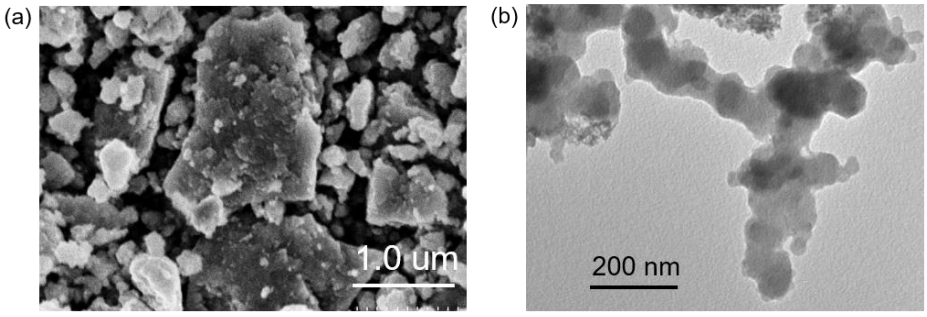

Figure S11. SEM and TEM of the prepared MnO_2 catalyst..

The images revealed that layered structure with different lateral size was obtained.

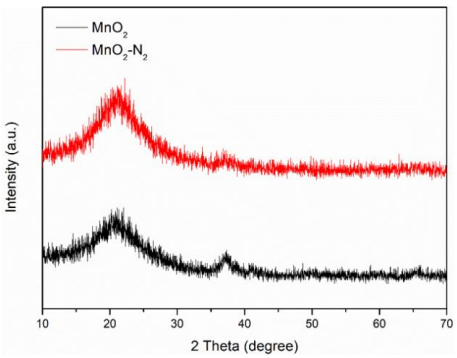

Figure S12. XRD pattern of the prepared MnO_2 catalyst.

The MnO_2 catalysts prepared by a solid interface reaction at room temperature showed a rather low crystallinity. After treatment under flow N_2 atmosphere at 200 °C for 2 h, the XRD patterns kept similar with the as-synthesized MnO_2 with no new patterns observed, demonstrating the treatment had no destructive impact on the bulk structure of the material.

2.6 The ECSA measurement of MnO_2 and MnO_2-N_2

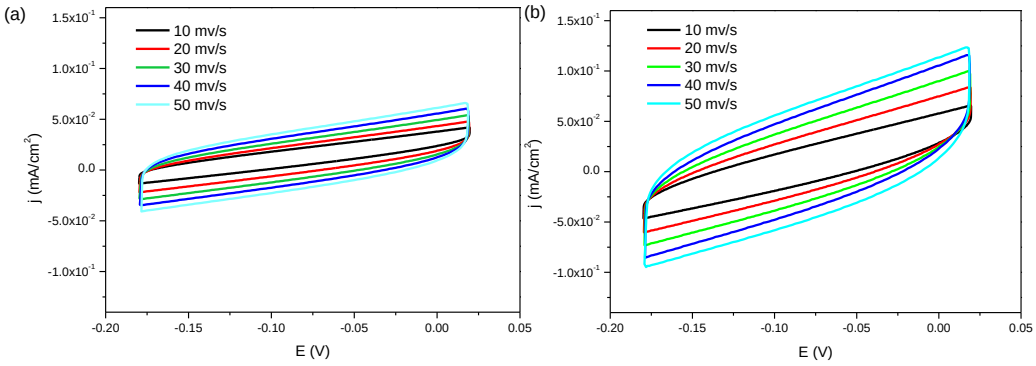

Figure S13. CVs at different scan rates of in a potential window where no Faradaic processes occur (-0.18~0.02 V vs.Fc/Fc^+) for MnO_2 and MnO_2-N_2 on CP. The calculation method for C_{dl} is shown in Experimental details.

2.7. Comparison of different anode materials for the electro-oxidation of THN

Table S3. Comparison of different different anod materials for the electro-oxidation of THN.

Entry	Anode	Potential (V)	Time (h)	Conv. (%)	Yield of TONE (%)	Yield of TOL (%)
1	MnO_2-CP	1.3	6	39.3	8.7	n.d.
2	MnO_2-CP	1.35	6	73.9	25.7	n.d.
3	MnO_2-CP	1.4	4.5	92.5	46.0	n.d.
4	MnO_2-N_2-CP	1.35	4.5	66.9	32.7	33.6
5	MnO_2-N_2-CP	1.35	6	82.5	40.6	16.2
6	MnO_2-CP	1.35	12	97.4	51.9	n.d.

[a] Reaction conditions: 0.65 mmol tetralin, cathode-Pt, 25 mL solvent (CH_3CN/H_2O=90/10)), electrolyte: 0.1 M Bu_4NClO_4, applied potential was vs Fc/ Fc^+; TONE and TOL are the abbreviation for 1-tetralone and 1-tetralol, respectively.

2.8 Characterization of catalyst after reaction

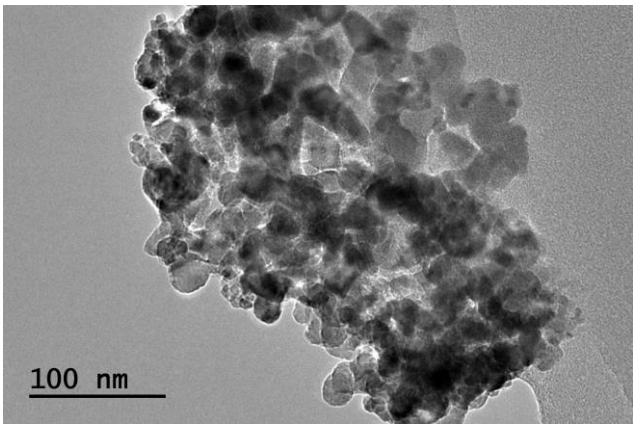

Figure S14. TEM image of the used MnO_2 catalyst.

The image revealed that the layered structure of catalyst after reaction was kept.

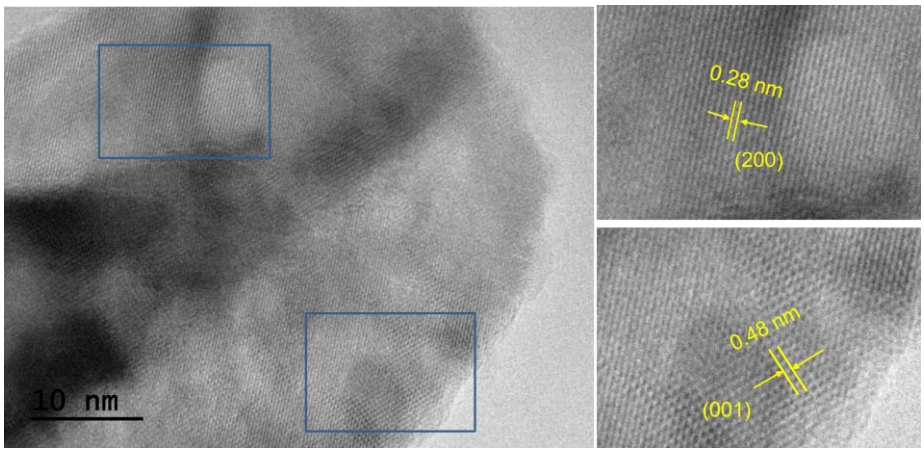

Figure S15. HRTEM image of the used MnO_2 catalyst.

Analysis of periodic lattice fringes in the High-resolution Transmission Electron Microscopy (HRTEM) image showed the same structural alignment.

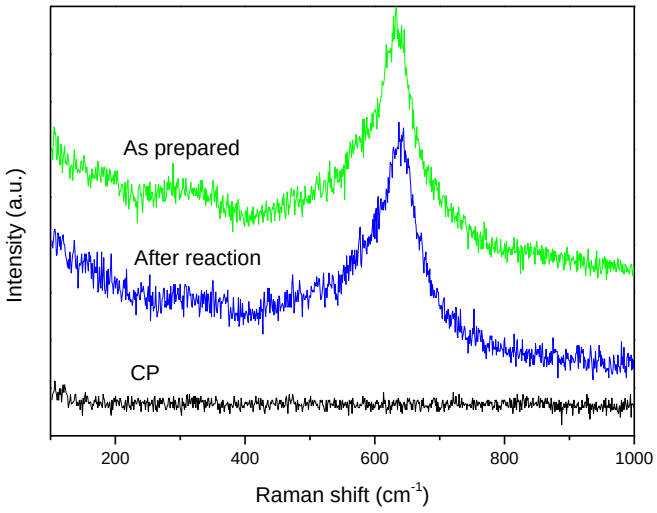

Figure S16. Raman spectra of the as-prepaared and used MnO_2-CP.

It is observed that the characteristic peak position at 638 cm-1 was kept, indicating the similar local atomic arrangements before and after reaction.

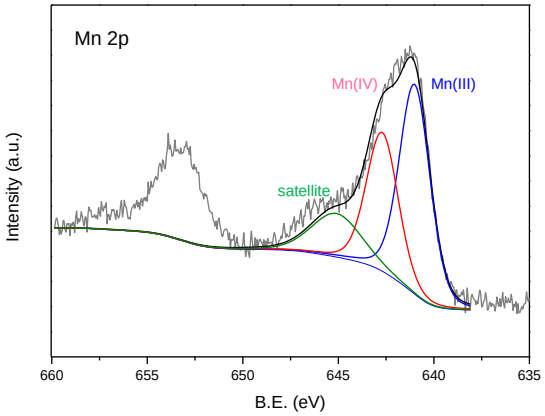

Figure S17. XPS spectrum of the used MnO_2-CP.

It is observed that the ratio of Mn(III) was higher that the as prepared sample, revealing that the local Mn sites on the catalyst surface went on some change to a degree (might originate from some MnOOH formation in water-involved reaction system)

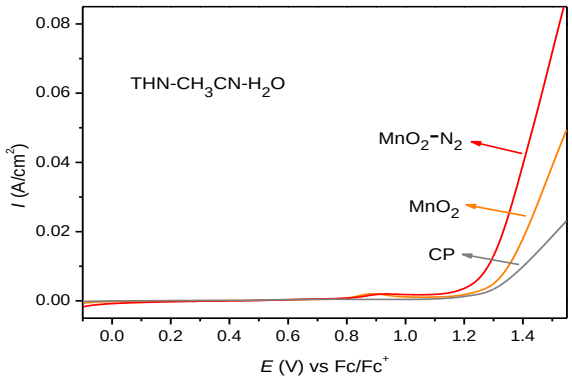

Figure S18. LSV plots of THN in CH_3CN-H_2O system, with MnO_2, MnO_2-N_2 deposited on CP and CP itself as anods.

2.9 CV plots of THN in different systems

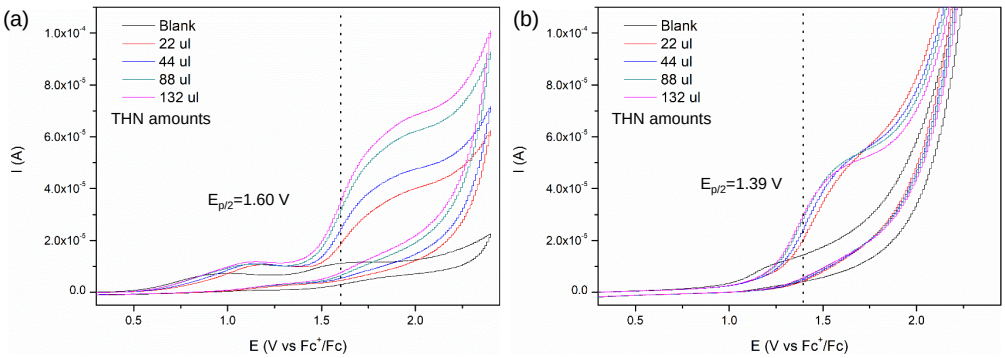

Figure S19. (a) CV of THN with different concentration in CH_3CN system, $E_{p/2}$=1.70 V. (b) CV of THN with different concentration in CH_3CN-H_2O system, $E_{p/2}$=1.49 V.

Electrolyte (Bu_4NClO_4, 0.1 M), solvent (25 mL), electrode (GC), the potential was calibrated by Fc/Fc^+.

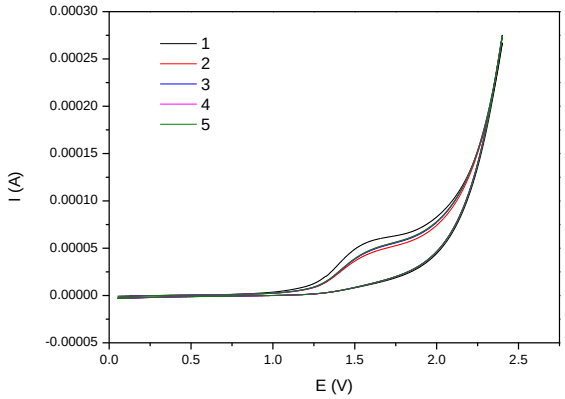

Figure S20. The CV plots for anodic reaction (1-5 cycles, until a stable current is achieved) .

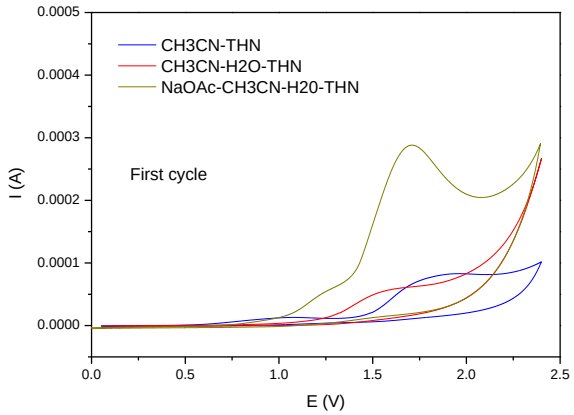

Figure S21. The first CV scan of THN in CH3CN (blue), CH_3CN-H_2O (red) and CH_3CN-H_2O system with addition of NaOAc (dark yellow).

2.10 The GC detection of O_2 gas in the system

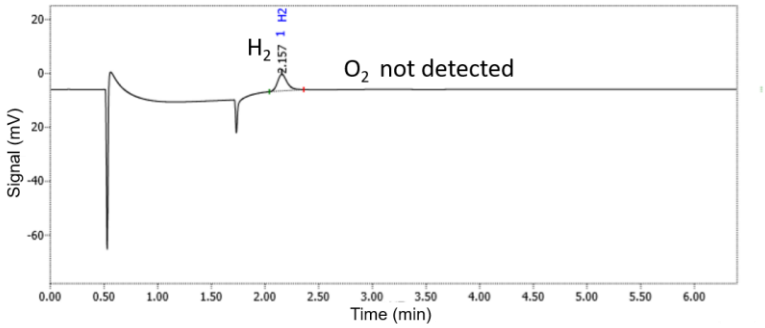

Figure S22. The GC chromatography for O_2 detection**.**

H_2 was obviously observed while the O_2 was almost indistinguishable. Considering extremely trace of O_2 evolution, the faradaic efficiency was not calculated.

2.11 The set up of the electrochemical cells

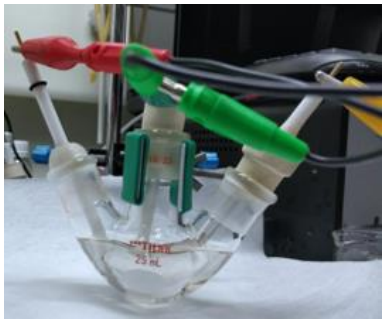

Figure S23. The digital graph of the setup of the electrochemical cell for Figure 1.

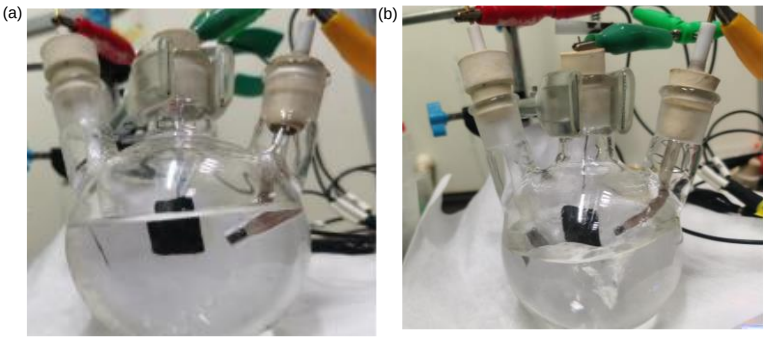

Figure S24. The digital graph of the setup of the scale-up experiment.

2.12 Information of isolated benzyl compounds

All ^{1}H NMR and ^{13}C NMR spectra of the products except for product 5h were measured in $CDCl_3$ using tetramethylsilane ((δ 0.00 for ^{1}H and ^{13}C) as an internal standard. Data are reported as follows: chemical shift in ppm (δ), multiplicity (s=singlet, d=doublet, t=triplet, m=multiplet), coupling constant (Hz), and integration.

1-Tetralone

^{1}H NMR (400 MHz, Chloroform-*d*) δ 8.04 (d, *J* = 7.8 Hz, 1H), 7.45-7.49 (m, 1H), 7.30-7.34 (m, 1H), 7.26 (d, *J* = 7.7 Hz, 1H), 2.97 (t, *J* = 6.1 Hz, 2H), 2.66 (t, 2H), 2.11-2.18 (m, 2H).
^{13}C NMR (100 MHz, Chloroform-*d*) δ 198.3, 144.5, 133.4, 132.6, 128.8, 127.2, 126.6, 39.2, 29.7, 23.3.

6-Methoxytetralone

^{1}H NMR (400 MHz, Chloroform-*d*) δ 8.03 (d, *J* = 8.8 Hz, 1H), 6.79-6.89 (m, 1H), 6.73 (d, *J* = 2.5 Hz, 1H), 3.88 (s, 3H), 2.90-2.98 (m, 2H), 2.65-2.61 (m, 2H), 2.08-2.18 (m, 2H).
^{13}C NMR (100 MHz, Chloroform-*d*) δ 197.2, 163.6, 146.9, 129.7, 126.4, 113.0, 112.6, 55.4, 38.9, 30.2, 23.4.

1-Indanone

^{1}H NMR (400 MHz, Chloroform-*d*) δ 7.76 (d, *J* = 7.7 Hz, 1H), 7.59 (t, *J* = 7.4 Hz, 1H), 7.48 (d, *J* = 7.7 Hz, 1H), 7.37 (t, *J* = 7.4 Hz, 1H), 3.18-3.11 (m, 2H), 2.72-2.65 (m, 2H).
^{13}C NMR (100 MHz, Chloroform-*d*) δ 207.0, 155.1, 137.1, 134.6, 127.3, 126.7, 123.7, 36.2, 25.8.

Benzophenone

^{1}H NMR (400 MHz, Chloroform-*d*) δ 7.90-7.77 (m, 4H), 7.61 (t, *J* = 7.4 Hz, 2H), 7.51 (t, *J* = 7.6 Hz, 4H).
^{13}C NMR (100 MHz, Chloroform-*d*) δ 196.7, 137.7, 132.4, 130.0, 128.3.

2H-Bezofuran-3-one

^{1}H NMR (400 MHz, Chloroform-*d*) δ 7.74 – 7.58 (m, 2H), 7.20 – 7.07 (m, 2H), 4.64 (s, 2H).
^{13}C NMR (100 MHz, Chloroform-*d*) δ 199.85, 174.01, 137.85, 124.07, 121.98, 121.18, 113.65, 74.68.

(4-nitrophenyl)(phenyl)methanone

^{1}H NMR (400 MHz, Chloroform-*d*) δ 8.32-8.17 (m, 2 H), 7.95-7.81 (m, 2 H), 7.79-7.62 (m, 2 H), 7.61-7.54(m, 1 H), 7.49-7.40 (m, 2 H).
^{13}C NMR (100 MHz, Chloroform-*d*) δ 194.80, 149.86, 142.82, 136.19, 133.54, 130.70, 130.12, 128.70, 123.55.

Phenyl(pyridin-2-yl)methanone

^{1}H NMR (400 MHz, Chloroform-*d*) δ 8.75-8.60 (m, 1H), 8.07-7.95 (m, 3H), 7.91-7.79 (m, 1H), 7.62-7.53 (m, 1H), 7.50-7.40 (m, 3H).
^{13}C NMR (100 MHz, Chloroform-*d*) δ 193.95, 155.13, 148.54, 137.05, 136.27, 132.90, 130.95, 128.15, 126.13, 124.61

Anthracene-9,10-dione

^{1}H NMR (400 MHz, Chloroform-*d*) δ 8.39 – 8.29 (m, 4H), 7.87 – 7.78 (m, 4H).
^{13}C NMR (100 MHz, Chloroform-*d*) δ 183.18, 134.14, 133.53, 127.25.

9H-fluoren-9-one

^{1}H NMR (400 MHz, Chloroform-*d*) δ 7.57 (d, J = 7.3 Hz, 2H), 7.44 – 7.37 (m, 4H), 7.20 (m, 2H).

^{13}C NMR (100 MHz, Chloroform-*d*) δ 193.96, 144.44, 134.70, 134.15, 129.08, 124.32, 120.32.

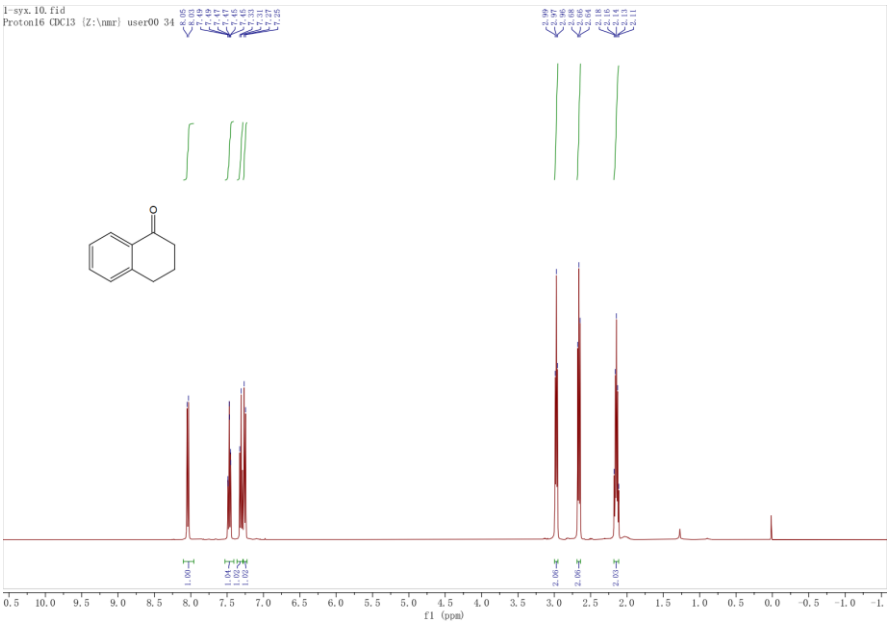

Figure S25. ^{1}H NMR of 1-Tetralone

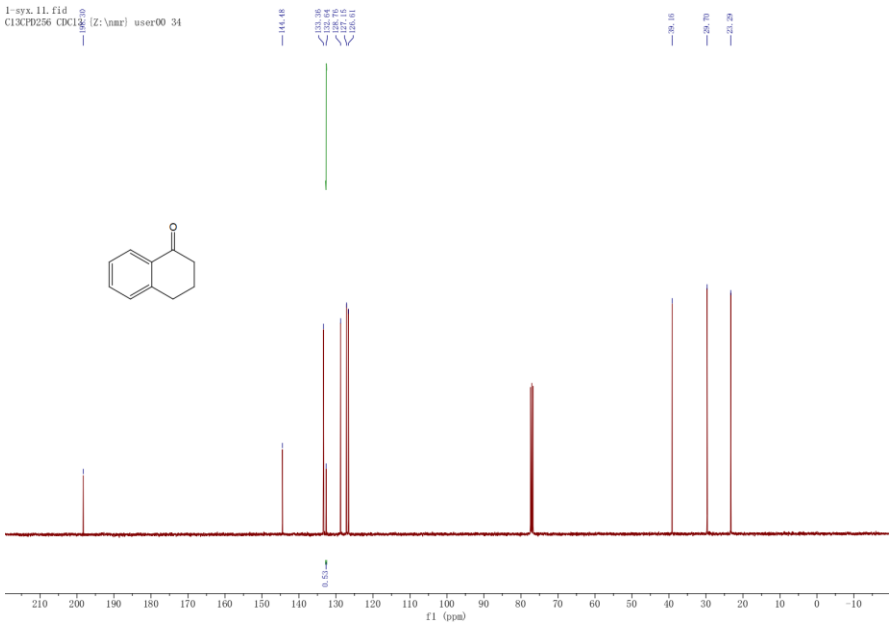

Figure S26. ^{13}C NMR of 1-Tetralone

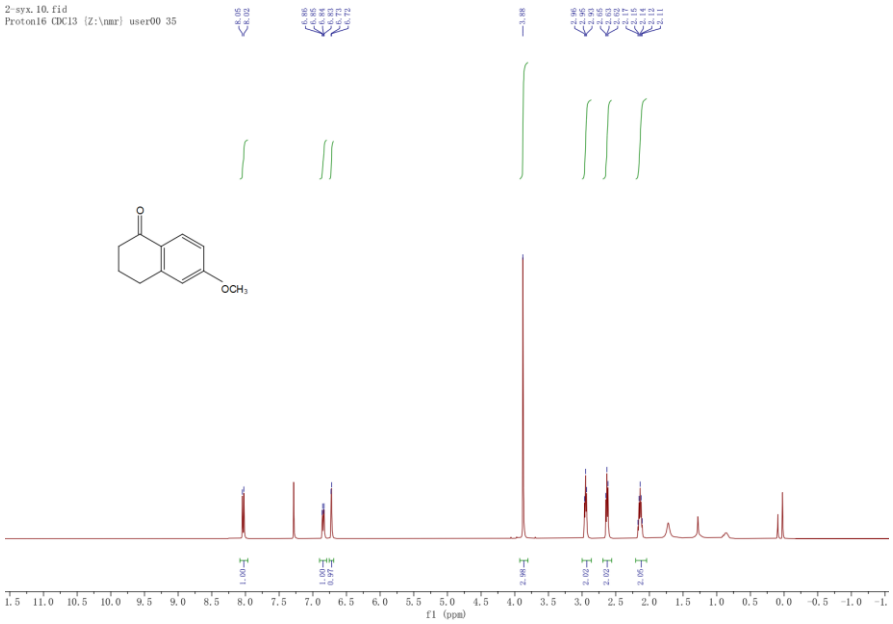

Figure S27. ^{1}H NMR of 6-Methoxytetralone

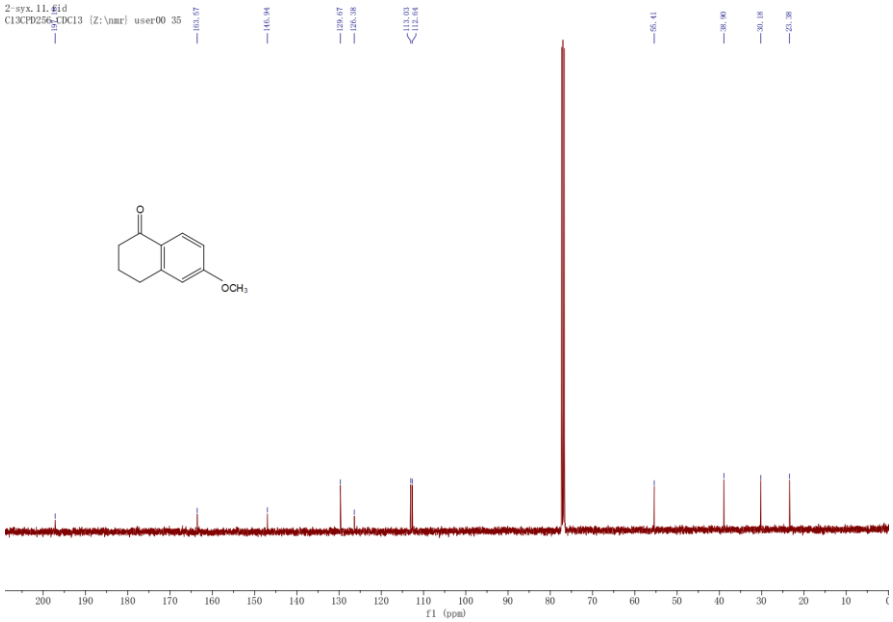

Figure S28. ^{13}C NMR of 6-Methoxytetralone

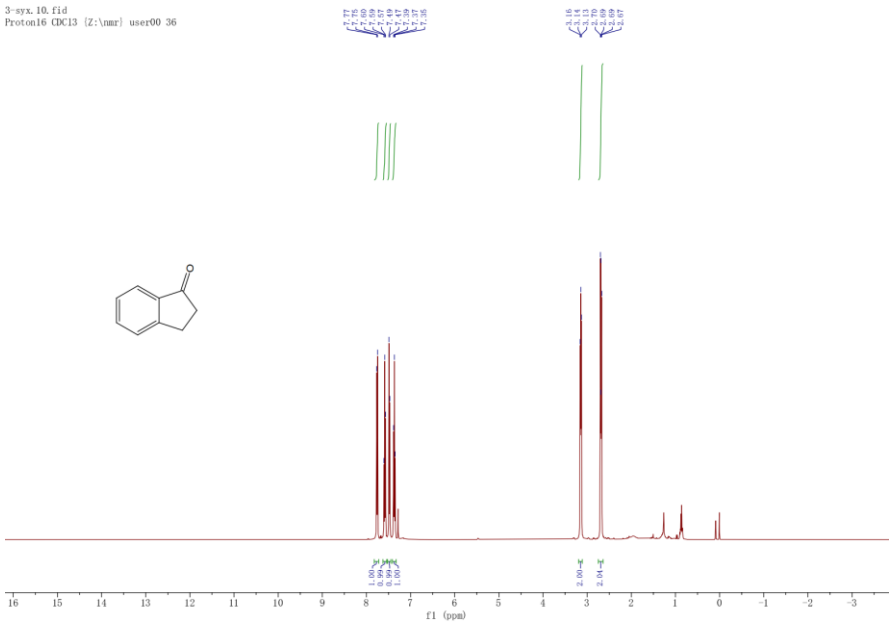

Figure S29. ^{1}H NMR of 1-Indanone

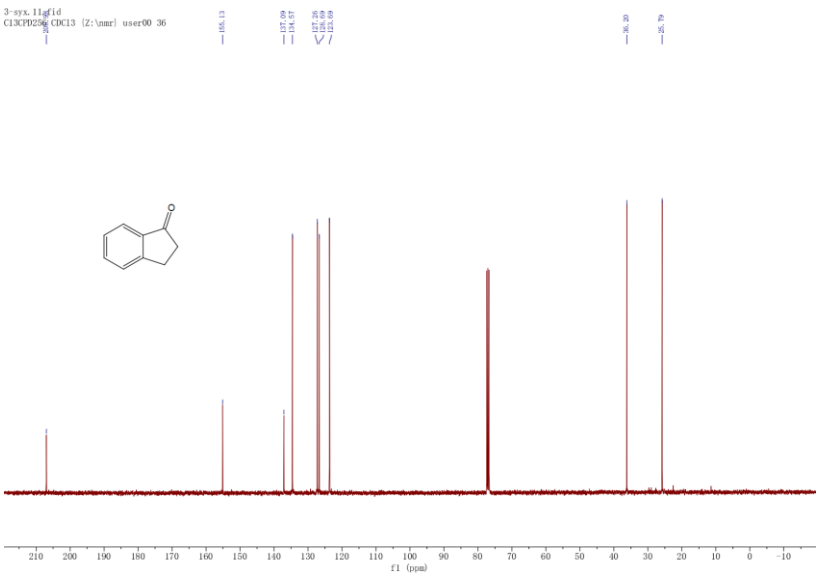

Figure S30. ^{13}C NMR of 1-Indanone

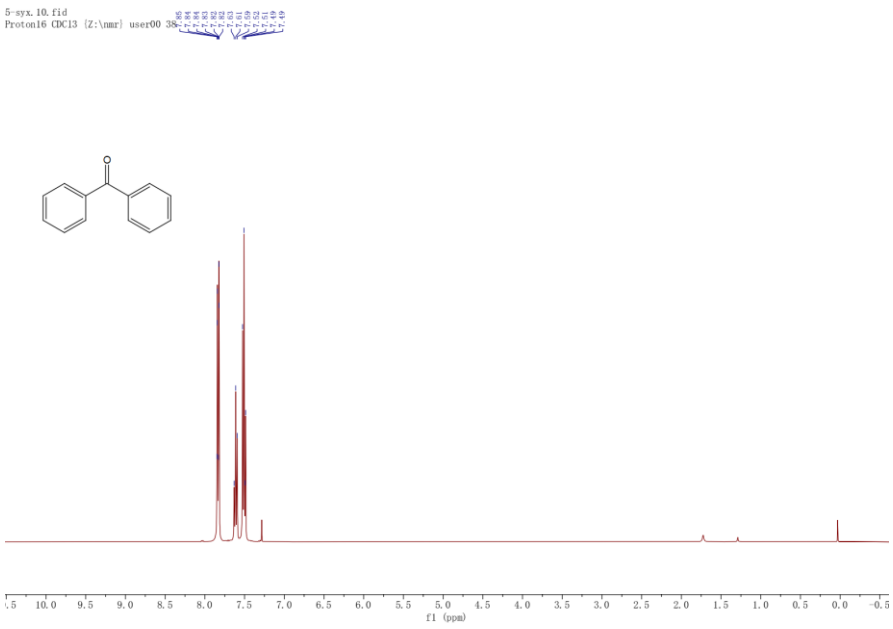

Figure S31. ^{1}H NMR of Benzophenone

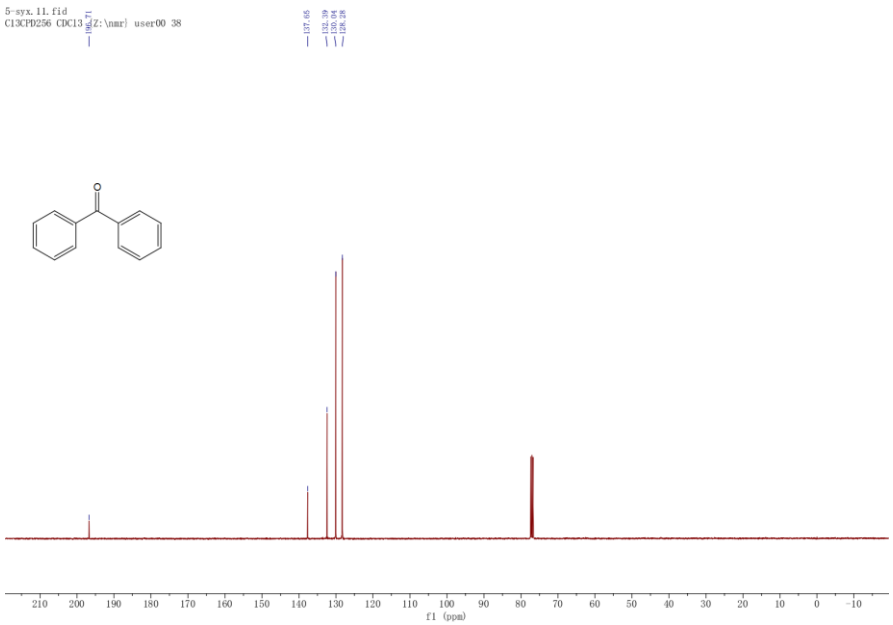

Figure S32. ^{13}C NMR of Benzophenone

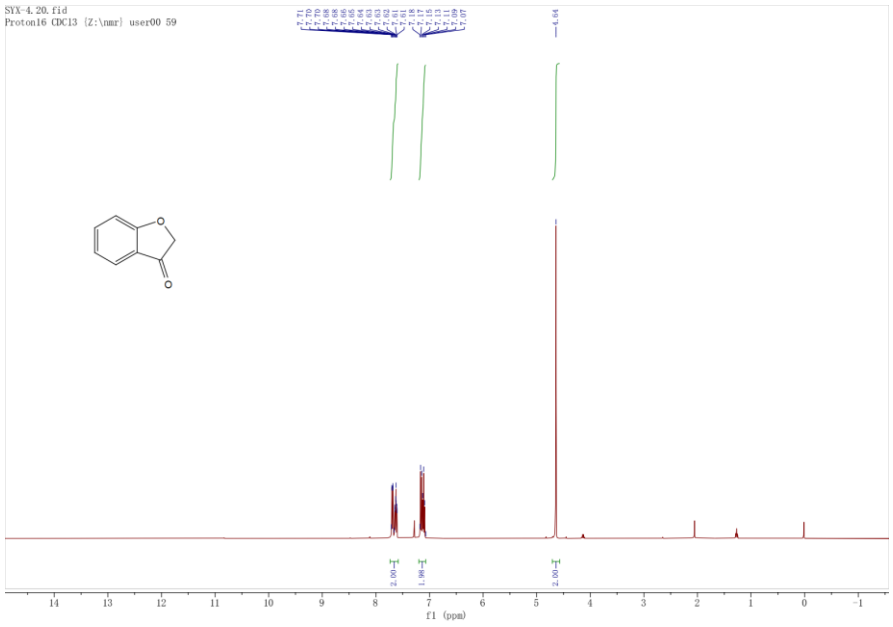

Figure S33. ^{1}H NMR of 2H-Bezofuran-3-one

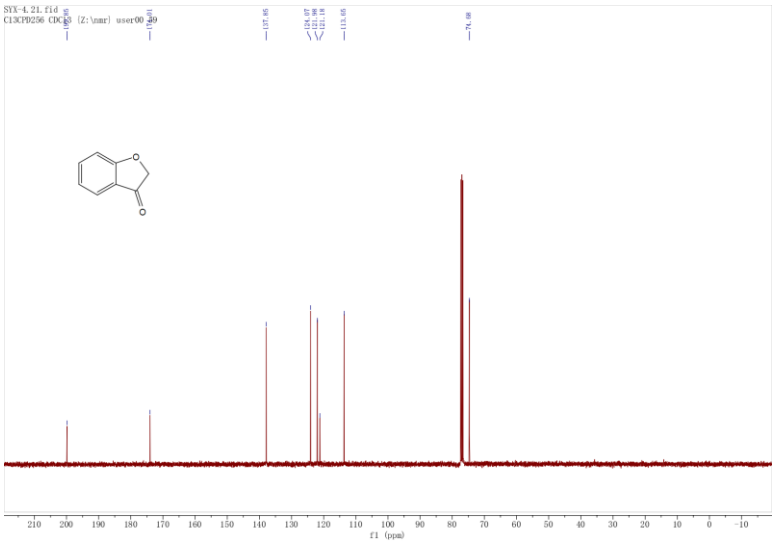

Figure S34. ^{13}C NMR of 2H-Bezofuran-3-one

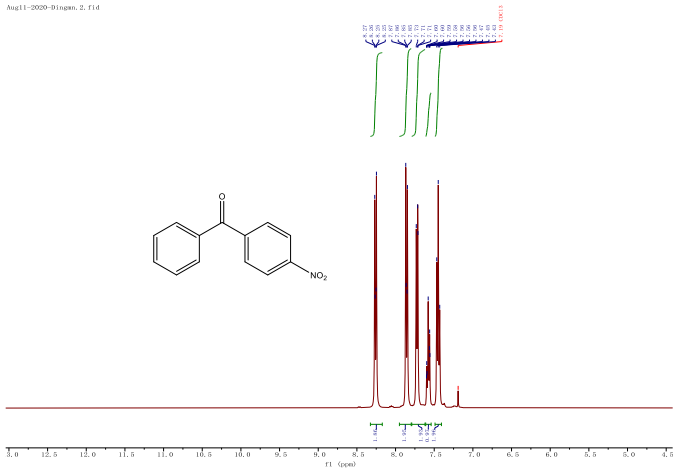

Figure S35. ^{1}H NMR of (4-nitrophenyl)(phenyl)methanone

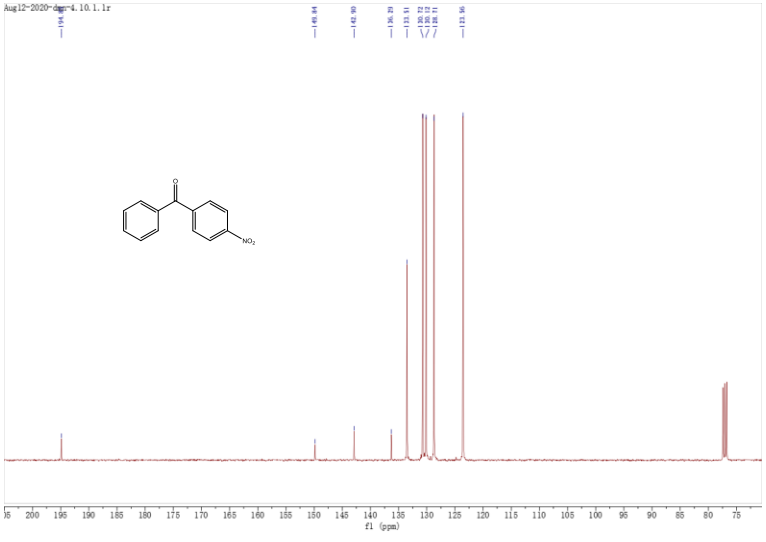

Figure S36. ^{13}C NMR of (4-nitrophenyl)(phenyl)methanone

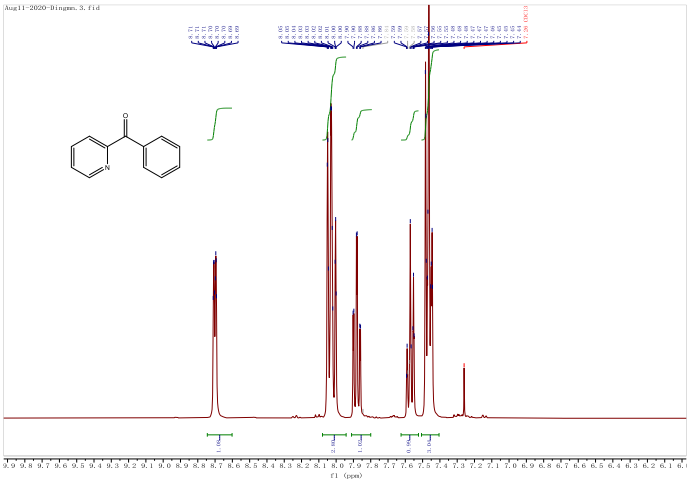

Figure S37. ^{1}H NMR of phenyl(pyridin-2-yl)methanone

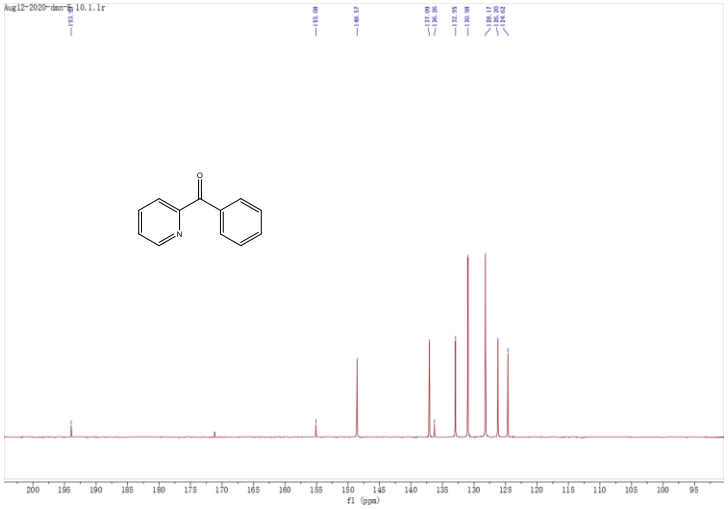

Figure S38. ^{13}C NMR of phenyl(pyridin-2-yl)methanone

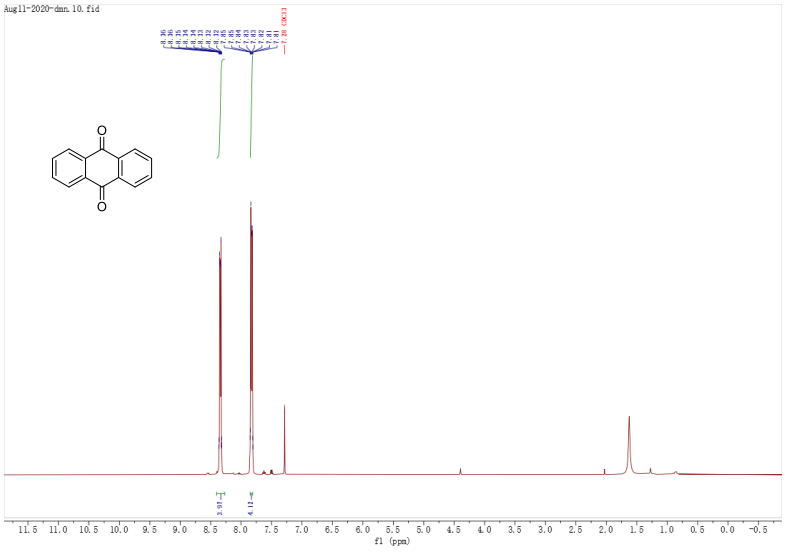

Figure S39. ^{1}H NMR of anthracene-9,10-dione

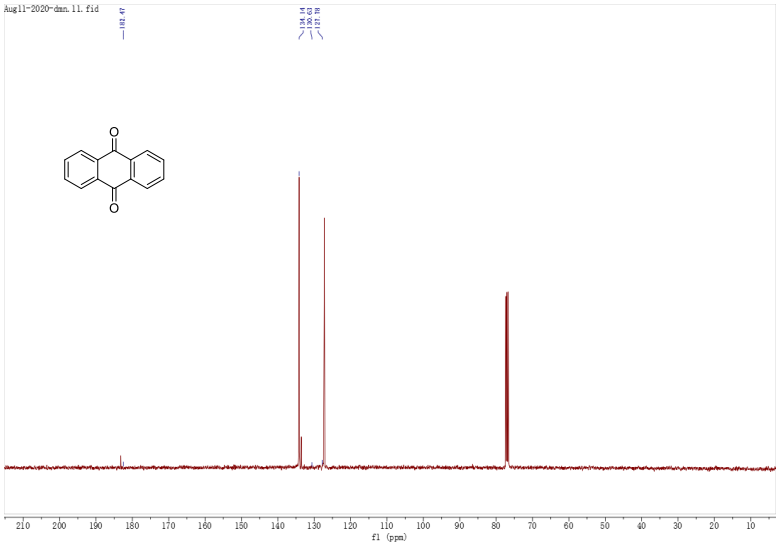

Figure S40. ^{13}C NMR of anthracene-9,10-dione

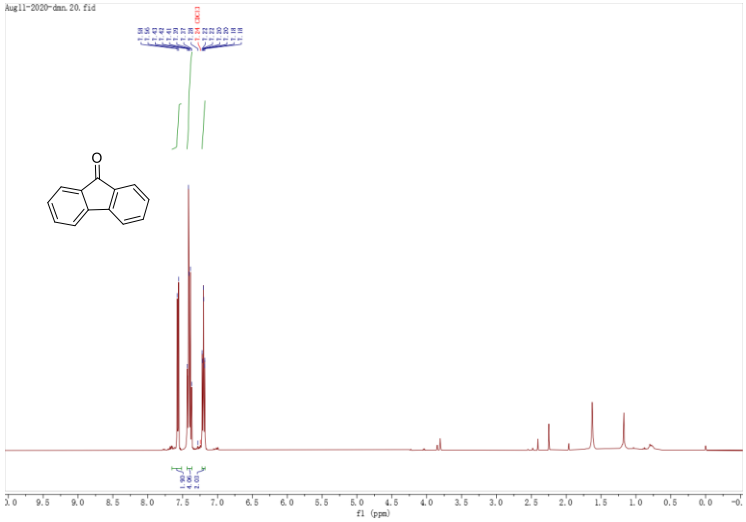

Figure S41. ^{1}H NMR of 9H-fluoren-9-one

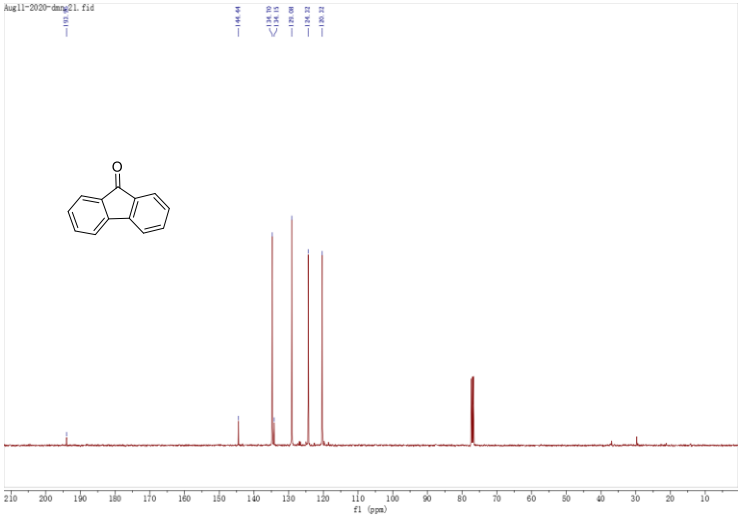

Figure S42. ^{13}C NMR of 9H-fluoren-9-one

3. References

[1] Liu, J.; Wei, Y.; Li, P. Z.; Zhang, P.; Su, W.; Sun, Y.; Zou, R.; Zhao, Y. Experimental and Theoretical Investigation of Mesoporous MnO2 Nanosheets with Oxygen Vacancies for High-Efficiency Catalytic DeNOx. *ACS Catal.* **2018**, *8*, 3865-3874.